THE JOURNAL OF PHYSICAL CHEMISTRY C LETTERS

2008, *112,* 12583–12589
Published on Web 07/26/2008

Effect of Polymer Nanoparticle Formation on the Efficiency of Polythiophene Based "Bulk-Heterojunction" Solar Cells

Adam J. Moulé,[†,§] Sybille Allard,[‡] Nils M. Kronenberg,[†] Argiri Tsami,[‡] Ullrich Scherf,[‡] and Klaus Meerholz*[,†]

Institut für Physikalische Chemie, Universität zu Köln, Luxemburgerstrasse 116, D-50939 Köln, Germany, and Macromolecular Chemistry Group and Institute for Polymer Technology, Bergische Universität Wuppertal, Gauss-Strasse 20, D-42097 Wuppertal, Germany

Received: May 15, 2008; Revised Manuscript Received: June 19, 2008

Polythiophenes are being intensively studied for use in polymer/fullerene bulk-heterojunction photovoltaic (PV) devices because they absorb light throughout the entire visible spectrum and show high hole mobility, which are the two most important parameters for a successful donor in these devices. A large body of anecdotal information exists about what morphological features lead to a high efficiency bulk-heterojunction PV device, but few design parameters for improved polymers exist. We compare two polythiophene isomers, poly(3-hexylthiophene) (P3HT) and poly(3,3‴-didodecylquaterthiophene) (PQT-12) to determine which parameters make these two polymers more and less suitable for use in bulk-heterojunction solar cells. We find that although they have nearly identical absorption spectra and hole mobilities, the PV devices made using P3HT are far superior to those made using PQT-12 because the PQT-12 forms crystalline nanoparticles in solution that do not form electrical connections in the thin films. The use of heat treatment for P3HT/fullerene films improves the layer morphology for PV applications but the same treatment for PQT-12/fullerene layers forces material separation on the micrometer length scale and further degradation of the electrical properties of the device.

1. Introduction

Recently, polymer−fullerene mixtures have been intensively studied for use in organic solar cells because they can be deposited from solution, are compatible with low-cost roll-to-roll fabrication technology, and have shown high power conversion efficiency (PCE), up to 4−5.5%.[1–4] The best single-layer devices consist of a bulk-heterojunction active layer, in which the polymer/donor and fullerene/acceptor are deposited from a common solvent.[5,6] As the solvent dries the donor and acceptor components separate into domains. Every fabrication parameter, including composition ratio,[7] deposition spinning speed,[8] polymer molecular weight (M_w),[9,10] heat treatment temperature[2,11] and choice of solvent,[12,13] has a large effect on the domain formation and, ultimately, the efficiency of the solar cell.[8] The PCE of the solar cell has been shown to be extremely sensitive to the size, composition and crystallinity of the formed domains.[8,14] To get beyond the "black magic" of finding recipes for efficient solar cells, we study here two different conjugated polythiophenes with identical formula weight but different domain forming properties. We look at each of these polymers in bulk-heterjunction solar cells with several M_w to try to determine which intrinsic properties are most pertinent for creating efficient devices.

In two recent studies, the influence of the formation of polymeric nanoparticles on the morphology of the bulk-heterojunction active layer of solar cells fabricated with mixtures of regioregular poly(3-hexylthiophene) (P3HT) and [6,6]-phenyl C_{61}-butyric acid methyl ester (PCBM) has been investigated. In the study by Berson et al., the authors were able to separate P3HT nanofibers from solvated P3HT in poor solvents.[15–17] The authors then made solar cells from predetermined mixtures of PCBM, solvated P3HT and P3HT nanofibers (P3HT-np). Using this technique, they were able to increase the as-cast efficiency of P3HT:PCBM solar cells from 0.65% to 3.6% by adding increasing percentages of P3HT-np to the casting mixture. Concurrently, our group performed a series of similar experiments with preformed P3HT-np solutions and also with methods for forming P3HT nanoparticles during the film formation process.[18] We obtained a similar increase in the efficiency of as-cast solar cells with added P3HT-np content.

The clear increase in the as-cast efficiency of polymer:PCBM solar cells led us to the question: is the formation of polymeric nanoparticles in solution, or during postproduction heat treatment necessary for making efficient bulk-heterojunction solar cells? To investigate this question, we use a comparison between the polymer donors P3HT and poly(3,3‴-didodecylquaterthiophene) (PQT-12) (Figure 1). Both polymers have been shown to have high field effect transistor (FET) mobilities of up to 0.1[19] and 0.14−0.2 $cm^2/(V^{-1}\ s^{-1})$,[20,21] respectively, depending on fabrication and tempering conditions. Even more interesting is that PQT-12 has also been shown to form stable nanoparticle suspensions at room temperature.[20] These nanoparticles self-

* To whom correspondence should be addressed. E-mail: Klaus.meerholz@uni-koeln.de.
† Universität zu Köln. E-mail: K.M., Klaus.meerholz@uni-koeln.de.
‡ Bergische Universität Wuppertal.
§ Current address: 1 Shields Ave., Chemical Engineering and Materials Science Department, University of California, Davis, Davis, CA 95616.

10.1021/jp8043016 CCC: $40.75

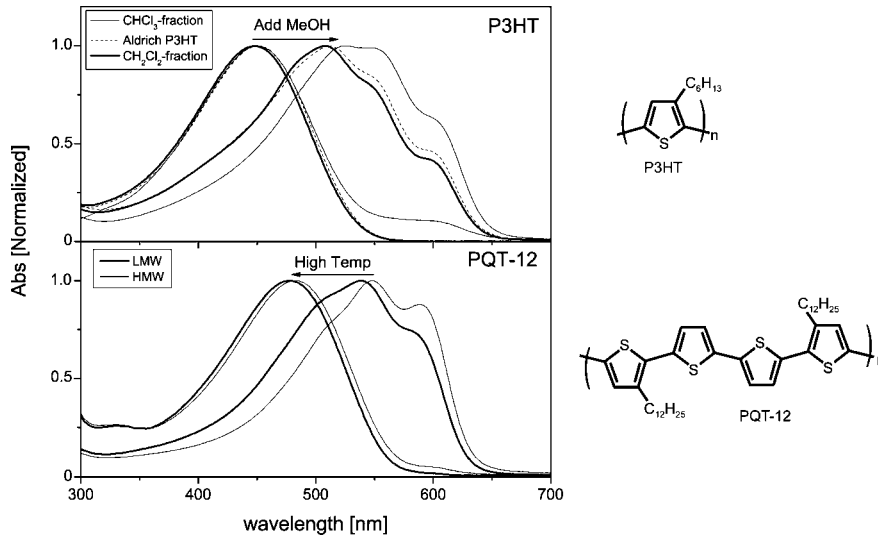

Figure 1. Absorption spectra of the materials used in this study. Top: solvatochromic shifts in the absorption spectra of Aldrich (dashed), $CHCl_3$ fraction (solid), and CH_2Cl_2 fraction (bold) P3HTs. The blue-shifted spectra are P3HT samples dissolved in $CHCl_3$ (as good solvent) and the red-shifted spectra are suspensions of P3HT nanoparticles after addition of methanol (1:9 $CHCl_3$:CH_3OH). Bottom: thermochromic shifts in the absorption spectra of LMW (bold) and HMW (solid) PQT-12 dissolved in chlorobenzene (CB). The red-shifted spectra were taken at room temperature and the blue-shifted spectra at 110 °C.

TABLE 1: Physical Properties of the Materials Used in This Study and of the Device Based on Them[a]

	P3HT				PQT-12	
	Aldrich	$CHCl_3$ frac	CH_2Cl_2 frac		LMW	HMW
M_w (g/mol)	50000	19200	11700		11200	47000
M_n (g/mol)	24000	14000	9100		9500	39000
PCBM wt %	35	45	35	45	80	80
J_{sc} [mA/cm^2]	11.18	11.39	10.96	9.98	4.31	4.30
V_{oc} [V]	0.65	0.61	0.64	0.66	0.61	0.54
FF	0.57	0.62	0.56	0.60	0.44	0.36
PCE [%]	4.10	4.33	3.96	3.96	1.15	0.83
peak ratio	1:0.90:0.61	1:0.96:0.71	1:0.93:0.66	1:0.90:0.63	1:0.76:0.45	1:0.78:0.46

[a] M_w, M_n, PCBM wt %, *IV* curve parameters, and absorption peak ratio of the polythiophene at 514, 550 and 601 nm (for P3HT) and 510, 548 and 589 nm (for PQT-12) for the best polythiophene:PCBM bulk-heterojunction devices produced.

assemble into stacked domains when spin coated onto Si substrates. PQT-12 has an identical formula weight to P3HT and similar HOMO and LUMO levels, which means that the bulk-heterojunction devices can be expected to have a similar open circuit voltage (V_{oc}) and charge-separation probability at polymer:PCBM interfaces. PQT-12 has already been investigated for use in polymer solar cells and compared to another substituted thiophene polymer.[22] We make a comparison between P3HT and PQT-12 to make generalizations about the necessary properties of donor polymers in bulk-heterojunction PV devices. We also investigate the influence of M_w on the ability of these polymers to form nanoparticle networks and, therefore, efficient bulk-heterojunction solar cells.

2. Experimental Details

P3HT was prepared with the so-called Grignard Metathesis (GRIM) procedure developed by McCullough et al.[23] PQT-12 was synthesized by oxidative coupling of the corresponding quaterthiophene monomer (3,3‴-didodecylquaterthiophene) according to the method of Ong et al.[24] The generation of P3HT and PQT-12 fractions of different molecular weights followed the so-called solvent extraction method as described by Pron et al.[25] for P3HT (the solvent extraction method has been used by other researchers to isolate a series of P3HT fractions for OFET mobility studies).[26,27] The molecular weights of the polymers were determined by gel permeation chromatography (GPC) using narrowly distributed polystyrene (PS) standards. Our study used a commercial P3HT sample (Aldrich-P3HT) as well as two P3HT batches made by solvent extraction with methylene chloride (CH_2Cl_2 fraction) and chloroform ($CHCl_3$ fraction). All of the low molecular weight material was first extracted with ethyl acetate (for the molecular weight data of the samples see Table 1). NMR measurements of the three samples indicated that the regio-regularity of the samples was nearly identical and >98%. Two PQT-12 samples were made by similar solvent extraction with methylene chloride and chloroform: a high molecular weight HMW (M_w = 47000 g/mol and M_n = 39000 g/mol) and low molecular weight LMW (M_w = 11200 g/mol and M_n = 9500 g/mol) sample.

All of the devices were fabricated by spin coating a polymer:PCBM layer onto an ITO-PEDOT:PSS substrate. The substrates were prepared as has previously been published.[7] The active layer was spin coated in a N_2 glovebox and then transferred to a high vacuum chamber where a Ca/Ag 6 nm/150 nm electrode was evaporated onto the sample. The device *IV* characteristics were measured using AM1.5 light and a Keithley 2425 source measurement unit in a N_2 glovebox. The intensity of the AM1.5 light was determined using a calibrated solar cell from the Fraunhofer Institute for solar research in Freiburg and a

reference P3HT:PCBM cell measured by the same institution. UV/vis spectra were taken with a Varian Cary 50 spectrometer.

3. Results and Discussion

Solvatochromic effects of P3HT in solvent/nonsolvent mixtures were first published by Bouman et al. using chloroform ($CHCl_3$) and methanol (MeOH).[28] This experiment has been repeated here for each of the three P3HT samples in Figure 1. The P3HT was dissolved at low concentration into $CHCl_3$ and a UV/vis spectrum was taken of P3HT in a disordered and nonstacked environment. Then MeOH as nonsolvent was added to the solution, which caused the P3HT to form nanoparticles. A UV/vis spectrum was then taken of the stable dispersion, which gives a measure of the degree of stacking that occurs, with the assumption that a 9:1 MeOH:$CHCl_3$ suspension is composed of 100% nanoparticle (solid state) P3HT.

Figure 1 depicts the absorption spectra of the P3HT and PQT-12 fractions that were investigated in our study. Compared with the other two fractions, the $CHCl_3$ fraction P3HT displays a higher crystallinity of the nanoparticles, as indicated by the increased size of the peak at 600 nm and the reduction of the disordered absorption shoulder at 450 nm. Interestingly, the solution absorption spectrum (recorded in chloroform) of the $CHCl_3$ fraction already exhibits some aggregate formation, as indicated by the long wavelength absorption shoulder up to 650 nm. This is surprising because this fraction possesses only a moderate molecular weight M_w of 19000 g/mol compared with the M_w of 50000 g/mol of the Aldrich-P3HT. The reason for this behavior is the much narrower molecular weight distribution of the $CHCl_3$ fraction, which better supports aggregate formation.

A similar experiment was performed for the two PQT-12 samples, LMW and HMW. In Figure 1 the thermochromic properties of both PQT-12 samples are shown. Because PQT-12 has a stronger particle-forming tendency than P3HT, chlorobenzene (CB) was used as the solvent. The PQT-12 could only be dissolved at elevated temperatures (see blue-shifted spectra). At a temperature of >110 °C and low concentrations, the PQT-12 nanoparticles are mainly dissolved. In this case, the UV/vis spectra are similar to the amorphous P3HT spectra and have an absorption maximum at ~480 nm. The spectrum of the HWM sample has a small shoulder at 589 nm, which corresponds to some undissolved (dispersed) PQT-12.

With reduced temperature, this shoulder quickly grows and the "nanoparticle-type" spectrum is recovered. At room temperature and low concentrations (0.01 mg/mL) PQT-12 forms stable nanoparticle dispersions, as is seen by the obvious color change of the solution (red-shifted spectra). Both the dispersions of the HMW and LMW samples show well-defined peaks at 589 and 548 nm with a shoulder at 510 nm. The peaks are located at almost identical wavelengths with respect to P3HT, but the peak ratios are decidedly shifted toward an increased lower energy contribution, which is an indication of increased crystalline content. In addition, the HMW sample shows a greater red shift and increased absorption at 589 nm compared with the LMW sample, which indicates that the HMW PQT-12 sample forms particles with higher crystallinity.

The average size of the particles in the dispersions was measured with a particle-sizer (dynamic light scattering). For this measurement, the assumption of a spherical particle is made. But, as has previously been shown, P3HT and PQT-12 preferentially form fibers.[15,16,20] The measurement, therefore, does not give an absolute size measurement, but rather a measure of the relative particle sizes. All three P3HT samples show particle sizes with a narrow distribution peaking at diameters of 30−40 nm for a solution concentration of 0.01 mg/mL in a $CHCl_3$:MeOH 1:9 mixture. Considering that the three samples have different M_w's, it is noteworthy that the particle sizes are nearly identical. We tested to see whether the average particle diameter is concentration dependent. A particle size measurement at higher P3HT concentration (0.025 mg/mL) exhibits increased average particle sizes of 40−50 nm diameter for all P3HTs. For the two PQT-12 samples, the dispersions of the LMW fraction shows an average particle diameter of 60 nm at a polymer concentration of 0.01 mg/mL. The HMW dispersion shows an increased particle diameter. Even 30 min after the solution of the HMW PQT-12 had been brought to room temperature, the particles continued to grow. We stopped measuring at a particle diameter of 250 nm. This indicates that the HMW PQT-12 sample displays a much greater tendency to form extended aggregates than the LMW sample.

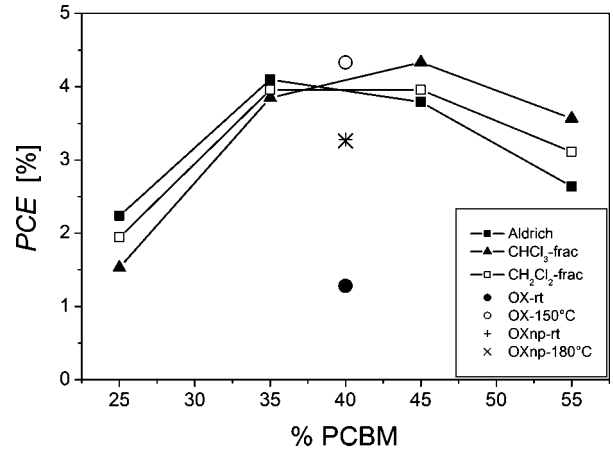

Figure 2. Power conversion efficiency under AM1.5 illumination for P3HT/PCBM devices as a function of PCBM wt % for the Aldrich P3HT (●), $CHCl_3$ fraction (▲) and CH_2Cl_2 fraction (□). Also depicted are the PCEs for as-cast (●, +) and heat-treated (□, ×) devices cast from *o*-xylene (OX) and from OX solutions with preformed P3HT nanoparticles (OXnp), respectively.

Next we made bulk-heterojunction polymer:PCBM solar cell devices. The P3HT-based devices for all M_w's were spincast using CB as the casting solvent. In this solvent the P3HT is completely dissolved. After evaporation of the Ca/Ag electrode, the samples were tempered at 150 °C for 10 min in a N_2 glovebox. The device active layer thickness was controlled to 80 ± 5 nm for all devices. Figure 2 shows a plot of PCE vs PCBM weight percentage (wt %). Both the CH_2Cl_2 fraction and the Aldrich P3HT samples have a PCE maximum at 35 PCBM wt % whereas the $CHCl_3$ fraction P3HT has its PCE maximum at 45 PCBM wt % (see Table 1 for full *IV* details). The significance of the maximum in PCE vs PCBM wt % can be summarized as follows. For a given layer thickness, the light capture in the active layer is increased with increasing P3HT because P3HT has a much higher absorption coefficient than PCBM over the solar spectrum. At the same time, increasing the P3HT content over a certain limit reduces the connectivity of the electron-transporting (PCBM-rich) phase (more and more isolated domains are formed), which reduces the internal quantum efficiency (IQE) and the filling factor (FF). The FF for a given polymer/PCBM combination is maximized by achieving a balance between hole and electron transport[29] and by achieving a morphology that allows both exciton separation and charge transport to each of the two electrodes.[30] The PCE maximum, therefore, marks the concentration ratio that balances light capture and electrical efficiency in P3HT:PCBM bulk-heterojunction devices.

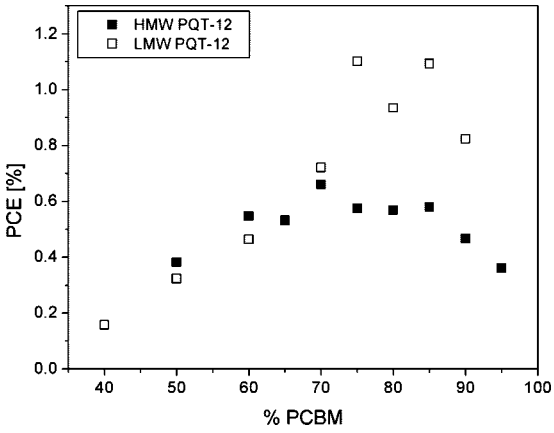

Figure 3. Power conversion efficiency under AM1.5 illumination for LMW (●) and HMW (□) PQT-12/PCBM bulk-heterojunction solar cells as a function of PCBM wt %.

Comparing the three P3HT fractions, the $CHCl_3$ fraction forms domains with higher crystallinity than the other two fractions (Figure 1), causing better hole-transporting properties. Therefore, a more balanced charge transport is realized and the efficiency peak is found for a higher PCBM concentration than for the other two samples. The higher crystallinity in the blend layers can be derived by comparing the UV/vis peak ratios at 514, 550 and 601 nm in P3HT/PCBM blends (Table 1; see Supporting Information Figure S1 for full spectra). Here, the intensity of the 601 nm peak increases with increasing crystallinity. The $CHCl_3$ fraction P3HT reaches an optimum PCE of 4.33% with maximized short circuit current J_{sc} and FF.

Looking at only these results, it would seem that increasing the crystallinity of P3HT in the active layer always increases the efficiency of the resulting PV device. However, Berson et al. have recently shown, by filtering pure P3HT nanofibers out of nanoparticle suspensions, that the device efficiency is higher when ~20% of the P3HT content in the active layer is amorphous because the amorphous P3HT creates pathways for holes between nanofiber hole-carrying domains.[15] It was also recently shown that the device efficiency is increased if the P3HT forms hole-carrying networks during the drying process, because this ensures the formation of three-dimensional, rather than one-dimensional conduction pathways.[18] For the record efficiency P3HT-based devices, either heat-tempering[2] or solvent-curing[1] is applied to generate an optimized morphology of the active layer.

Also depicted in Figure 2 are as-cast and heat-treated P3HT:PCBM bulk-heterojunction devices (40 wt % PCBM) fabricated from fully dissolved Aldrich P3HT and from preformed P3HT nanoparticle dispersions (P3HT-np) in *o*-xylene (OX). The fabrication of these devices has been described elsewhere.[18] Here it can be clearly seen that the as-cast device made from preformed nanoparticles shows a much improved PCE of 3.3% compared with the device with fully dissolved, amorphous P3HT (1.2%). This is because the preformed nanoparticles guarantee a much higher hole mobility within the preformed crystalline domains. After heat treatment, however, the device cast from fully dissolved, amorphous P3HT shows a high efficiency of 4.3%, where the efficiency of the device cast from preformed nanoparticles (P3HT-np) remains at 3.3%. (Note: The 4.3% efficiency result was taken from a different Aldrich P3HT batch and recorded on a different day. Each P3HT batch has a unique polydispersity that can greatly affect device efficiency. Also, the calibration error on the AM1.5 illumination was ±5%. For these reasons, this result cannot be directly compared to the other Aldrich P3HT results shown here. Finally, calculation of efficiency does not include a correction for spectral mismatch.) This result shows that inclusion of the preformed nanoparticles supports the formation of high hole-mobility domains, but the ultimate efficiency is limited because of the large diameter of the initial P3HT nanoparticles of 30−40 nm. The data on P3HT-np was previously published.[18]

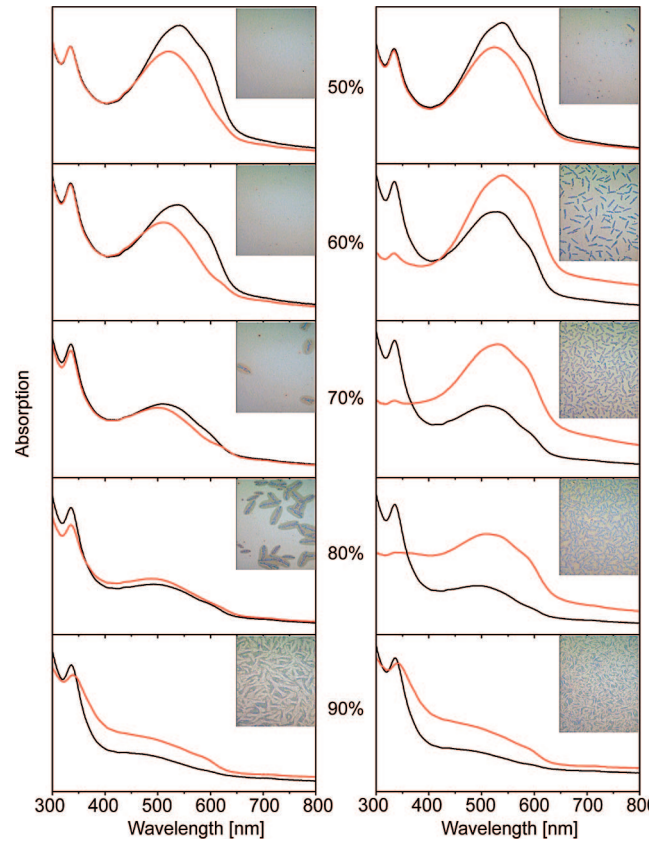

Figure 4. UV/vis spectra of HMW (right) and LMW (left) PQT-12/PCBM thin-film layers spin cast from 1,2-dichlorobenzene. Depicted are the spectra of as-cast layers (black) and the same layers after heat treatment at 150 °C for 10 min (red). Reflection optical microscopy images are included for the heat-treated samples as insets (area 1 × 1 mm^2). The weight percentages indicate the PCBM content.

We also made PQT-12:PCBM bulk-heterojunction-type solar cells based on both samples (LMW/HMW) (Figure 3). Room temperature deposition means that the PQT-12 is actually a nanoparticle dispersion at the time of spin coating. But, because particle size measurements showed that the particle size is not stable, the solutions were heated overnight and brought to room temperature directly before spin coating. The particle size of the HMW sample cannot be estimated. Figure 3 shows the PCE vs wt % PCBM for HMW and LMW PQT-12 devices. Devices were fabricated using both CB and *o*-dichlorobenzene (ODCB) as solvents, but because solvent choice made no significant difference (<10%) in any of the *IV* parameters, all devices were averaged together and each point is an average of 5−15 devices from both solvents. The highest PCE of ca. 1.2% was recorded for a device of 80 PCBM wt % and using the LMW PQT-12 polymer. This comparatively low PCE was due to both low J_{sc} and low FF. The requirement of high PCBM content and the observation of low FF are usually associated with a low hole mobility.[31] It has, however, been shown that PQT-12:PCBM devices with similar component ratios have a comparable space-charge-limited-current (SCLC) hole mobility to P3HT/PCBM mixtures.[22]

SCHEME 1: PQT-12 Film Features for (Left) Randomly Oriented Nanoparticle Domains in an As-Cast Film and (Right) the Formation of Larger Domains Oriented with the Substrate Surface for Heat-Treated Films[a]

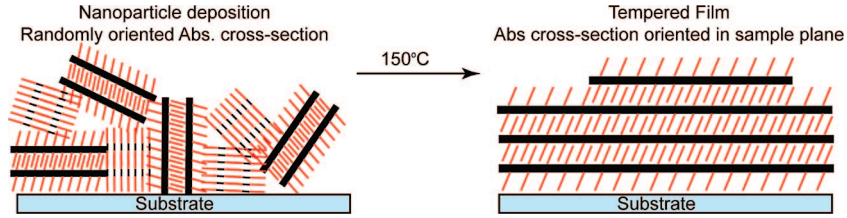

[a] The right image was reproduced from the publication of R. J. Kline et al.[35]

A second explanation for the low J_{sc} and FF is an unfavorable morphology. There are two potential problems with the PQT-12:PCBM morphology. First, the low J_{sc} could be caused by poor charge transfer between the PQT-12 and PCBM, which is caused by the formation of large PQT-12 domains with reduced interfacial area. Because charge transfer only occurs at the boundary between donor and acceptor materials and the exciton diffusion length is only 5−10 nm,[32] the formation of large PQT-12 (larger than 60 nm diameter; see above) domains would exclude the inner part of PQT-12 domains from charge transfer. This conclusion is supported by the result that devices made of HMW PQT-12, which form larger nanoparticle domains in solution, have lower J_{sc} and PCE than devices made from LMW PQT-12. Second, the PQT-12:PCBM distance could be increased due to the longer solublizing side chains (dodecyl), with respect to P3HT. Studies of PV devices made from mixtures of poly(3-dodecylthiophene) (P3DDT) with PCBM also showed roughened morphology and reduced efficiency.[33] The authors concluded, however, that reduced mutual solubility, not physical blocking due to increased side chain length, caused the efficiency reduction. Both this study and the study by Nguyen et al. suggest that formation of large PQT-12 domains that exclude PCBM are the source of the efficiency reduction.

Bulk-heterojunction PV devices that have a low FF usually have either a very low charge mobility or unbalanced mobility between charge species. Typically, the hole mobility is lower than the electron mobility. This difference in mobility leads to a buildup of holes within the active layer and ultimately to SCLC.[34] In the case of PQT-12 the hole mobility, as measured using field effect measurements, is quite high and should lead to a high FF. However, both fractions show a low FF of only 0.36 (HMW fraction) and 0.44 (LMW fraction). This low FF could be explained by poor connectivity between PQT-12 domains due to the lack of an amorphous "glue" between crystalline domains.

In contrast to P3HT/PCBM layers, heat treatment (150 °C) of PQT-12/PCBM devices led to a significant decrease in the PCE (>30%) for all devices. We also noticed that the UV/vis spectra of the heat-treated layers changed in unexpected ways. In the case of P3HT/PCBM layers it has been shown that heat treatment leads to the formation of crystalline domains: this is seen in the UV/vis spectrum as a red shift and the growth of vibronic character (peaks).[2,11] Heat treatment leads to an increased absorption and red shift for all mixing ratios of P3HT/PCBM with no change in spectrum outside of P3HT absorption. However, for PQT-12 layers and PQT-12/PCBM layers with a PCBM wt % less than 80% (LMW) and 60% (HMW), heat treatment of the layer led to a significant decrease in the absorption of the PQT-12 (Figure 4). In addition, the PQT-12 absorption looses vibronic character (defined peaks) and blue shifts.

For PCBM wt % equal to or greater than 80% (LMW) and 60% (HMW), the PQT-12 absorption increases with heat treatment. Also noteworthy in these spectra is that with increased PCBM wt %, heat treatment reduces the PCBM absorption. The change in the PCBM absorption can be explained by examination of the insets to the spectra, which are reflection optical microscopy images with 50-fold magnification of the heat-treated layers (see insets in Figure 4). With increased PCBM wt % and heat treatment, the PCBM phase separates from the layer upon heat treatment and forms aggregates that are large enough to scatter light. Short wavelength light is preferentially scattered in these aggregates. Simultaneously, the average PCBM content of the layer is reduced, which causes a decrease in the PCBM absorption with respect to the PQT-12 absorption. At very high PCBM loading, the PCBM absorption is restored because the entire film is covered in PCBM aggregates.

The change in the PQT-12 part of the spectrum with heat treatment is controlled not by aggregation, but by the orientation of the PQT-12 backbone with respect to the incident radiation. It has previously been shown that films of pure heat-treated PQT-12 orient into stacked interdigitated sheets with the π-stacking direction roughly parallel to the substrate plane.[35,36] In this orientation, the absorption coefficient is highly anisotropic, with absorption cross-section that is higher in the plane than perpendicular to the sample plane (Scheme 1b). However, because the films are spin-cast from PQT-12 nanoparticles, it can be expected that the orientation of the π-stacking is random due to the random orientation of the nanoparticles (Scheme 1a). Therefore, a UV/vis spectrum taken of the film before heat treatment will have an isotropic absorption coefficient. During heat treatment above the glass transition temperature, the PQT-12 domains orient with the substrate surface and become larger, so that after heat treatment the absorption coefficient is anisotropic and reduced perpendicular to the plane. This reduction is seen in the UV/vis spectra in Figure 4. The apparent blue shift in the UV/vis spectrum of PQT-12 is due to the relatively larger contribution of the PCBM component to the absorption.

For films in Figure 4 with high PCBM wt % loading, the PQT-12 portion of the UV/vis spectrum increases in absorption with heat treatment. We believe that the PQT-12 domains remain randomly oriented in the PCBM matrix with heat treatment, but that the scattering caused by agglomeration of the PCBM also increases the apparent absorption increase of the PQT-12.

Further evidence for the change from random, nanoparticle-triggered phase formation to organized, substrate-triggered phase formation of the PQT-12 films is seen in atomic force microscopy (AFM) images of PQT-12 films. Figure 5 shows tapping-mode topography and phase images of a LMW PQT-12 film before and after heat treatment at 150 °C for 10 min, respectively. The peak-to-valley roughness is nearly identical, but the heat-treated film clearly has a much larger average topological features, as one could expect from the data presented above. The phase images show differences in the "material hardness". The as-cast film was made from nanoparticles with

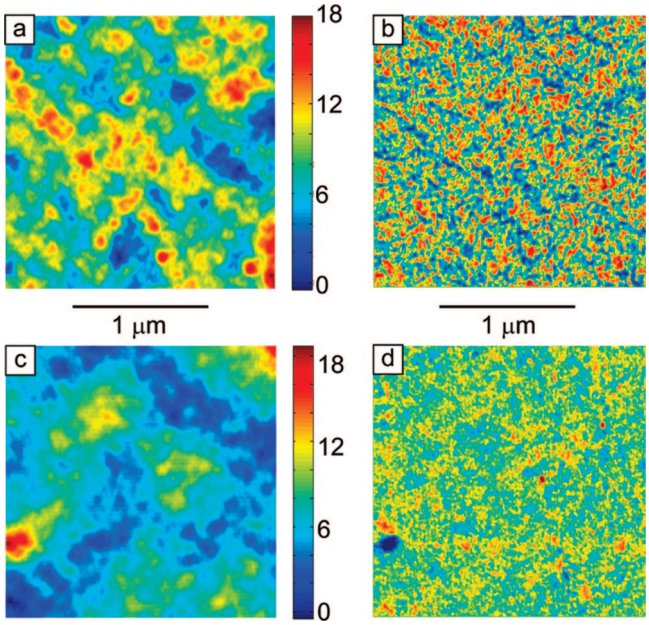

Figure 5. Tapping-mode AFM images Topography (a, c) and phase (b, d) of as-cast (a, b) and heat-treated (c, d) LMW PQT-12 films, respectively. The length scale is depicted as a bar. Both phase images use an identical color code.

a large variety of orientations with respect to the exposed surface. This is reflected in the extremes of the color scale (blue and red). The heat-treated film has more uniformly oriented domains, which is reflected in the constant middle (yellow to green) color distribution.

We reasoned that we could improve the device efficiency by reducing the aggregated content in the PQT-12 portion of the mixed PQT-12/PCBM films so that the PQT-12 domains were connected by amorphous polymer strands as is seen in P3HT/PCBM films. As a test of this idea, we fabricated LMW PQT-12:PCBM blend layers from 150 °C solutions of ODCB. At low concentrations these hot solutions showed an amorphous UV/vis spectrum, indicating that nanoparticles were not present in solution (see Figure 1). However, the higher concentration solutions necessary for device fabrication were black rather than orange, which indicates that nanoparticles were still preformed in the solution. Devices fabricated from these hot solutions had a lower efficiency (J_{sc} = 3.45 mA/cm,^{2} V_{oc} = 0.69 V, FF = 0.35, PCE = 0.8%) than devices cast from room temperature solutions (see Supporting Information Figure S2). The increased V_{oc} and reduced FF in the hot-cast PQT-12:PCBM devices were typical of untempered P3HT:PCBM devices. When the hot-cast devices were heat-treated, crystallization of PCBM still occurred, but on a much lower and slower scale than for the room temperature cast devices. This shows that increasing the casting temperature did cause the two components to mix more intimately, but the tendency of PQT-12 to form particles is still too strong for making good solar cells.

4. Conclusions

We have made a comparison of the polythiophene isomers P3HT and PQT-12 for use in polymer:PCBM bulk-heterojunction solar cells. Our investigation used samples of differing molecular weights to investigate the molecular weight influence on the layer morphology and to give us clues into how the realized morphology affects the device power conversion efficiency. For the P3HT-based devices power-conversion efficiencies of up to 4.3% were recorded. The moderate molecular weight P3HT fraction ($CHCl_3$ fraction) of narrow polydispersity produced the best device and this was shown to be because this P3HT fraction displayed the highest degree of crystallinity, with an optimum PCE of 4.33% for a PCBM loading of 45 wt %. In contrast to P3HT, PQT-12 forms nanoparticle dispersions at room temperature solution. Devices made from mixtures of PQT-12 and PCBM therefore contain preformed nanoparticles that cause mesoscopically demixed blends with low charge-separation efficiency. We conclude that the size of the crystalline polymer domains (preformed or formed during postprocessing treatments) is critical for good charge transport in bulk-heterojunction solar cells. However, the amount of the amorphous matrix that acts as a kind of glue between the crystalline domains is also an important parameter. Active layers fabricated from preformed crystalline nanoparticles seem inappropriate for the formation of high-efficiency bulk-heterojunction solar cell devices, because the electronic connection between the individual polymer domains is insufficient.

Acknowledgment. We acknowledge the Alexander von Humboldt foundation for the post doctoral grant of AM. We also thank the German Ministry of Science and Education (BMBF) for funding EKOS project (O3N2023D) and the Ministry of Science and Innovation of Northrhine-Westfalia (Elena-project). We thank David M. Huang for discussion and editing.

Supporting Information Available: UV/vis absorption spectra and *IV* curves. This material is available free of charge via the Internet at http://pubs.acs.org.

References and Notes

(1) Li, G.; Shrotriya, V.; Huang, J.; Yao, Y.; Moriarty, T.; Emery, K.; Yang, Y. *Nat. Mater.* **2005**, *4*, 864.
(2) Ma, W.; Yang, C.; Gong, X.; Lee, K.; Heeger, A. J. *Adv. Funct. Mater.* **2005**, *15*, 1617.
(3) Reyes-Reyes, M.; Kim, K.; Carroll, D. L. *Appl. Phys. Lett.* **2005**, *87*, 083506.
(4) Peet, J.; Kim, J. Y.; Coates, N. E.; Ma, W. L.; Moses, D.; Heeger, A. J.; Bazan, G. C. *Nat. Mater.* **2007**, *6*, 497.
(5) Halls, J. J. M.; Walsh, C. A.; Greenham, N. C.; Marseglia, E. A.; Friend, R. H.; Moratti, S. C.; Holmes, A. B. *Nature* **1995**, *376*, 498.
(6) Yu, G.; Gao, J.; Hummelen, J. C.; Wudl, F.; Heeger, A. J. *Science* **1995**, *270*, 1789.
(7) Moulé, A. J.; Bonekamp, J. B.; Meerholz, K. *J. Appl. Phys.* **2006**, *100*, 094503.
(8) Hoppe, H.; Sariciftci, N. S. *J. Mater. Chem.* **2006**, *16*, 45.
(9) Schilinsky, P.; Asawapirom, U.; Scherf, U.; Biele, M.; Brabec, C. J. *Chem. Mater.* **2005**, *17*, 2175.
(10) Hiorns, R. C.; De Bettignies, R.; Leroy, J.; Bailly, S.; Firon, M.; Sentein, C.; Khoukh, A.; Preud'homme, H.; Dagron-Lartigau, C. *Adv. Funct. Mater.* **2006**, *16*, 2263.
(11) Padinger, F.; Rittberger, R. S.; Sariciftci, N. S. *Adv. Funct. Mater.* **2003**, *13*, 85.
(12) Shaheen, S. E.; Brabec, C. J.; Sariciftci, N. S.; Padinger, F.; Fromherz, T.; Hummelen, J. C. *Appl. Phys. Lett.* **2001**, *78*, 841.
(13) Rispens, M. T.; Meetsma, A.; Rittberger, R.; Brabec, C. J.; Sariciftci, N. S.; Hummelen, J. C. *Chem. Commun.* **2003**, 2116.
(14) Halls, J. J. M.; Arias, A. C.; MacKenzie, J. D.; Wu, W. S.; Inbasekaran, M.; Woo, E. P.; Friend, R. H. *Adv. Mater.* **2000**, *12*, 498.
(15) Berson, S.; De Bettignies, R.; Bailly, S.; Guillerez, S. *Adv. Funct. Mater.* **2007**, *17*, 1377.
(16) Ihn, K. J.; Moulton, J.; Smith, P. *J. Polym. Sci., Part B-Polym. Phys.* **1993**, *31*, 735.
(17) Merlo, J. A.; Frisbie, C. D. *J. Polym. Sci., Part B-Polym. Phys.* **2003**, *41*, 2674.
(18) Moulé, A. J.; Meerholz, K. *Adv. Mater.* **2008**, *20*, 240.
(19) Sirringhaus, H.; Brown, P. J.; Friend, R. H.; Nielsen, M. M.; Bechgaard, K.; Langeveld-Voss, B. M. W.; Spiering, A. J. H.; Janssen, R. A. J.; Meijer, E. W.; Herwig, P.; de Leeuw, D. M. *Nature* **1999**, *401*, 685.
(20) Ong, B. S.; Wu, Y. L.; Liu, P.; Gardner, S. *Adv. Mater.* **2005**, *17*, 1141.

(21) Salleo, A.; Chen, T. W.; Volkel, A. R.; Wu, Y.; Liu, P.; Ong, B. S.; Street, R. A. *Phys. Rev. B* **2004**, *70*, 115311.
(22) Thompson, B. C.; Kim, B. J.; Kavulak, D. F.; Sivula, K.; Mauldin, C.; J., F. c., J. M .*Macromolecules* **2007**, *40*, 7425.
(23) Loewe, R. S.; Khersonsky, S. M.; D, M. R. *Adv. Mater.* **1999**, *11*, 250.
(24) Ong, B. S.; Wu, Y. L.; Liu, P.; Gardner, S. *J. Am. Chem. Soc.* **2004**, *126*, 3378.
(25) Trznadel, M.; Pron, A.; Zagorska, M. *Macromolecules* **1998**, *31*, 5051.
(26) Zen, A.; Pflaum, J.; Hirschmann, S.; Zhuang, W.; Jaiser, F.; Asawapirom, U.; Rabe, J. P.; Scherf, U.; Neher, D. *Adv. Funct. Mater.* **2004**, *14*, 757.
(27) Kline, R. J.; McGehee, M. D.; Kadnikova, E. N.; Liu, J. S.; Frechet, J. M. J. *Adv. Mater.* **2003**, *15*, 1519.
(28) Bouman, M. M.; Havinga, E. E.; Janssen, R. A. J.; Meijer, E. W. *Mol. Cryst. Liq. Cryst. Sci. Technol. Sect. a-Mol. Cryst. Liq. Cryst.* **1994**, *256*, 439.
(29) Mihailetchi, V. D.; Xie, H. X.; de Boer, B.; Koster, L. J. A.; Blom, P. W. M. *Adv. Funct. Mater.* **2006**, *16*, 699.
(30) van Duren, J. K. J.; Yang, X. N.; Loos, J.; Bulle-Lieuwma, C. W. T.; Sieval, A. B.; Hummelen, J. C.; Janssen, R. A. J. *Adv. Funct. Mater.* **2004**, *14*, 425.
(31) Melzer, C.; Koop, E. J.; Mihailetchi, V. D.; Blom, P. W. M. *Adv. Funct. Mater.* **2004**, *14*, 865.
(32) Markov, D. E.; Amsterdam, E.; Blom, P. W. M.; Sieval, A. B.; Hummelen, J. C. *J. Phys. Chem. A* **2005**, *109*, 5266.
(33) Nguyen, L. H.; Hoppe, H.; Erb, T.; Gunes, S.; Gobsch, G.; Sariciftci, N. S. *Adv. Funct. Mater.* **2007**, *17*, 1071.
(34) Mihailetchi, V. D.; Koster, L. J. A.; Hummelen, J. C.; Blom, P. W. M. *Phys. Rev. Lett.* **2004**, *93*, 216601.
(35) Kline, R. J.; DeLongchamp, D. M.; Fischer, D. A.; Lin, E. K.; Richter, L. J.; Chabinyc, M. L.; Toney, M. F.; Heeney, M.; McCulloch, I. *Macromolecules* **2007**, *40*, 7960.
(36) Kline, R. J.; DeLongchamp, D. M.; Fischer, D. A.; Lin, E. K.; Heeney, M.; McCulloch, I.; Toney, M. F. *Appl. Phys. Lett.* **2007**, *90*, 3.

JP8043016